2-15-2019

Experimental Study: Underwater Propagation of Super-Gaussian and Multi-Gaussian Schell-model Partially Coherent Beams with Varying Degrees of Spatial Coherence

Svetlana Avramov-Zamurovic
United States Naval Academy

Charles L. Nelson
United States Naval Academy

Milo W. Hyde IV
Air Force Institute of Technology

Recommended Citation

S. Avramov-Zamurovic, C. Nelson, and M. Hyde, "Experimental study: underwater propagation of super-Gaussian and multi-Gaussian Schell-model partially coherent beams with varying degrees of spatial coherence," OSA Continuum 2, 450-459 (2019). https://doi.org/10.1364/OSAC.2.000450

Research Article Vol. 2, No. 2 / 15 February 2019 / OSA Continuum 450

Experimental study: underwater propagation of super-Gaussian and multi-Gaussian Schell-model partially coherent beams with varying degrees of spatial coherence

S. AVRAMOV-ZAMUROVIC,[1,*] C. NELSON,[2] AND M. HYDE[3]

[1] *Weapons, Robotics, and Control Engineering Department, US Naval Academy, 105 Maryland Avenue, Annapolis, MD 21402, USA*
[2] *Electrical and Computer Engineering Department, US Naval Academy, 105 Maryland Avenue, Annapolis, MD 21402, USA*
[3] *Air Force Institute of Technology, 2950 Hobson Way, Dayton, OH 45433, USA*
[*] *avramov@usna.edu*

Abstract: We report on experiments where super-Gaussian and flat-top, multi-Gaussian Schell-model spatially partially coherent beams, with varying degrees of spatial coherence, were propagated underwater. Two scenarios were explored—calm and mechanically agitated water. The main objective of our study was the experimental comparison of the scintillation statistics. For a similar degree of coherence widths, the results show a potentially improved performance of scintillation index for the multi-Gaussian Schell-model beams as compared to the super-Gaussian beams. It should be noted that the presented results pertain only to the given experimental scenarios and further investigation is necessary to determine the scope of the findings.

1. Introduction

Propagation of laser light, and laser light intensity fluctuations, through random media [1,2] is of great interest for laser applications. While much of the recent research has focused on laser propagation through turbulent atmospheric conditions, with an emphasis on scintillation mitigation by source partial coherence [3,4,5], aperture averaging [6], sparse aperture detectors [7,8], wavelength diversity [9], source temporal variations [10], and polarization diversity [11–14], the study of laser light propagation underwater is of emerging significance. This is predominately motivated by communication and sensing applications, in particular, with submersible robots [15–18]. That said, significant challenges remain in regards to light intensity distortion underwater which requires additional detailed study and exploration.

Light scintillation in the ocean has been theoretically studied for plane, spherical, and Gaussian beams [19], as well as for partially coherent beams [20]. Non-uniformly correlated partially coherent beams have also been recently studied [21–23]. Our motivation and interest is to experiment with source coherence as well as to explore alternate beam classes in an underwater medium.

In this experiment, we chose to explore the effects of an alternate window function with a similar degree of coherence width, but functionally raised to the fourth power, instead of the traditional square. We call these partially coherent beams, super Gaussian beams (SGs). The goal was to see if SG beams might propagate more effectively, judged by scintillation statistics, through a random underwater medium as compared to multi-Gaussian Schell-Model spatially partially coherent beams.

Multi-Gaussian Schell-model (MGSM) spatially partially coherent beams [24] have a flat-top intensity profile and can be created through a straightforward technique utilizing a spatial light

#353334 https://doi.org/10.1364/OSAC.2.000450
Journal © 2019 Received 4 Dec 2018; accepted 24 Dec 2018; published 11 Feb 2019

OSA CONTINUUM

modulator (SLM), which allows spatial degree of coherence manipulation. This technique also allows us to readily explore additional beam classes.

Our experiments explore laser light intensity fluctuations, when spatially partially coherent MGSM beams as well as SGs with varying degrees of coherence are propagated underwater in two different scenarios—calm and mechanically agitated water. Our findings indicate a potential scintillation index performance benefit of MGSM as compared with SG beam classes. To our knowledge, this paper is the first to report experimental results of partially spatially coherent beams propagating through underwater turbulence.

The paper is organized as follows: MSGM beam and SG generation is presented in Section 2. The experimental set-up is discussed in Section 3, followed by data analysis and results in Sections 4 and 5, respectively. Lastly, Section 6 concludes this paper.

2. Beam generation

2.1. Scalar MGSM beams

In this paper, we provide a brief overview of the theory behind the generation of MGSM beams, additional details can be found in Refs. [24–26]. A recently developed model for the MGSM (flat-top) beam, gives the following spectral degree of coherence:

$$\mu^{(0)}(\rho_1, \rho_2) = \frac{1}{C_0} \sum_{m=1}^{M} \begin{pmatrix} M \\ m \end{pmatrix} \frac{(-1)^{m-1}}{m} \exp\left[-\frac{|\rho_2 - \rho_1|^2}{2m\delta^2}\right], \tag{1}$$

where ρ_1 and ρ_2 are vector positions, superscript (0) refers to the source plane,

$$C_0 = \sum_{m=1}^{M} \begin{pmatrix} M \\ m \end{pmatrix} \frac{(-1)^{m-1}}{m} \tag{2}$$

is a normalization factor to ensure that the spectral degree of coherence is unity at the origin, and $\begin{pmatrix} M \\ m \end{pmatrix}$ is the binomial coefficient. In Eq. (1), δ is the r.m.s. correlation width which is a measure of the spatial coherence of the beam: $\delta = 0$ models a spatially incoherent beam and $\delta \rightarrow \infty$ models a spatially coherent beam. Additionally, the upper index M relates to the flatness of the intensity profile in the far field: $M = 1$ corresponds to the classic Gaussian Schell-model (GSM) source, and $M \rightarrow \infty$ corresponds to a flat-topped, hard-edged, far-zone intensity profile.

Reference [24] provides general details on how one uses Eqs. (1) and (2) to generate MGSM beams using an SLM. Additionally, the SLM phase screens were augmented with a grating to shift the zeroth-order "hot spot" off of the beam propagation path [27–30].

2.2. Scalar super Gaussian beams

We propose the following super Gaussian (SG) experimental window function and explore the performance relative to GSM and MGSM beams with similar r.m.s. correlation widths:

$$\mu SG^{(0)}(\rho_1, \rho_2) = \exp\left[-\frac{|\rho_2 - \rho_1|^4}{2\delta^4}\right], \tag{3}$$

where the variables are the same as defined in Eqs. (1) and (2). The significant difference here is that the magnitude of the vector position differences is raised to the fourth power instead of squared. Figure 1 shows plots of the window functions given in Eqs. (1) and (3) for $\delta = 0.19$ mm. Note that even though the beam classes have the same δ, the radii of the window functions (see

OSA CONTINUUM

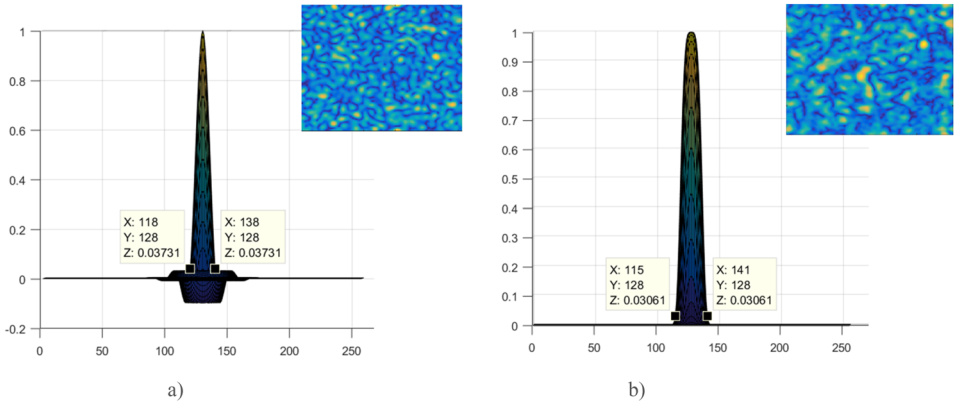

Fig. 1. Representative source window functions and example phase screens (top right corners) for a) MGSM beam and b) SG beam as a function of SLM pixel number with $\delta = 0.19$ mm. Note that even though $\delta = 0.19$ mm, the beam radii for the MGSM beam is 0.24 mm and 0.31 mm for the SG beam.

Fig. 1) are a bit different—for the MGSM beam its 0.24 mm and for the SG beam its 0.34 mm. This is a by-product of the beams having differently shaped correlation functions.

The effective width of the window function determines the coherence width of spatially partially coherent beam. In this sense a wider width translates to a more spatially coherent beam, and thus a beam that is generally more susceptible to the influence of turbulence.

3. Experimental set-up

As shown in Fig. 2, a stabilized 2 mW, 632.8 nm He-Ne laser, A, was expanded, B, to fill a 256×256 (6.14 mm $\times$ 6.14 mm) SLM, C. To eliminate the zeroth-order "hot spot" produced by the SLM, a $4f$ system with two 400 mm lenses, E_1 and E_2, and a mechanical iris, F, were used to isolate the desired first diffraction order and block the rest. A linear polarizer, D_1, was used to align the linear polarization state of the laser with the SLM's control state, vertical in this case, and a linear polarizer, D_2, was used following the SLM to maintain the vertical polarization (previous experimentation showed a slight polarization rotation following the SLM). A shearing interferometer was used to verify collimated light was incident on the SLM and exited the $4f$ system. After passing through the $4f$ system, the light propagated approximately 5 m via a mirror, G_1, and a 90:10 beam splitter, H, before entering the water tank, I.

The water tank, I, was 76 cm long by 30 cm wide and filled with approximately 38 liters of distilled water. The water was kept at room temperature (approximately 20 °C). A mechanical agitator moved the water to create turbulence during the experiments.

The laser light intensity fluctuations were recorded using two cameras, J_1 and J_2, where J_1 was positioned on-axis, after reflection from mirror G_2, with neutral density filters to prevent saturation. The second camera, J_2, was positioned perpendicularly to the primary beam path and was used to capture the laser light intensity fluctuations and intensity before entering the water tank. Each camera had a sensor with a 14-bit resolution and was 480×640 pixels (7.4 µm pitch) yielding a total active area of 3.552 mm $\times$ 4.736 mm.

The spatial coherence radii tested in the experiments ranged from 0.19 mm to 0.54 mm and 8,000 screens for each source [see Eqs. (1) and (3)] and each coherence radius, cycling at a rate of 333 Hz, were used to synthesize the partially coherent beams. For each data run, J_1 and J_2 captured approximately 500 images at a rate of 10 Hz, with an exposure time of 100 ms. This

OSA CONTINUUM

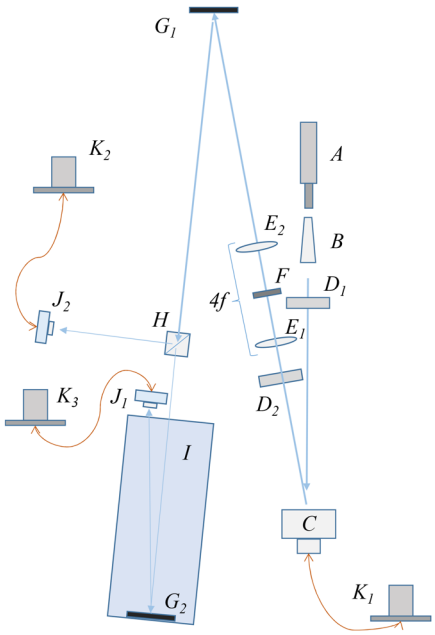

Fig. 2. Experimental set-up - A – He-Ne laser, B – beam expander, C – spatial light modulator, $D_{1,2}$ – linear polarizer, $E_{1,2}$ – lenses with focal lengths of 400 mm, F – mechanical iris (placed at the focal planes of $E_{1,2}$), $G_{1,2}$ – mirrors, H – beam splitter, I – water tank, $J_{1,2}$ – cameras, $K_{1,2,3}$ – computers.

frame rate and exposure time ensured that approximately 30 SLM frames were integrated per collected image, thus providing reasonable theoretical conditions for the analysis of partially coherent beams [31].

4. Data analysis

As done in Ref. [32] and described here for clarity, the focus of our data analysis is to explore the s variance of light over the sensor area.

The first step is the computation of the mean scattered intensities I_{avg} for beams propagating through the water. It is important to note that the background noise has been eliminated from all of the analysed images. Assuming that each image (im) is an m x n matrix, with $m = 480$ and $n = 640$, and that there are $N = 500$ images, we find the I_{avg} as

$$I_{avg} = \frac{\sum_{j=1}^{N} (im)_j}{N}. \tag{4}$$

The spatial variance of the intensity fluctuations across the sensor area with the background B_{avg} removed is calculated as

$$SI_B = \frac{\frac{\sum_{i=1}^{N} ((im_i - B_{avg}) - (I_{avg} - B_{avg}))^2}{N}}{(I_{avg} - B_{avg})^2}, \tag{5}$$

where B_{avg} is a single parameter representing the average background intensity. Note that SI_B is the background removed scintillation index. To obtain a single parameter representing Eq. (5),

OSA CONTINUUM

we find the spatially averaged value of SI_B, namely,

$$MSI_{B\,avg} = \frac{\sum_{k=1}^{n} \sum_{j=1}^{m} SI_B[j,k]}{nm}. \tag{6}$$

An example of the measured intensity and the scintillation index for an SG beam propagating in calm water is shown in Fig. 3, and as expected there is very little scintillation across the profile. The scintillation index for each pixel is given (see Fig. 3b) and the range of values shows uncorrelated measurements in relation to measured intensity.

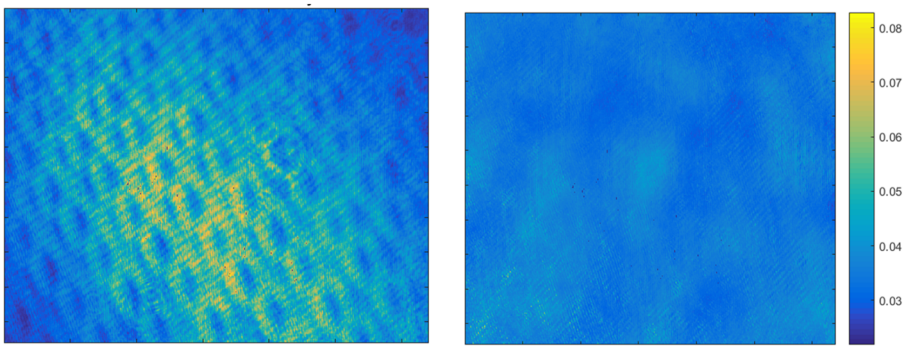

Fig. 3. Example measured values of a) mean light intensity I_{avg} and b) scintillation index SI_B for the SG beam with $\delta = 0.38$ mm in calm water across the sensor area (3.552 mm × 4.736 mm).

Additionally, due to image artefacts and varying experimental conditions we opted to use thresholding to capture the representative performance of the beam on propagation axis.

The following method was used for the thresholding, first we find the highest value of the measured average intensity I_{max}, (for example see Fig. 3). The time series intensity variations at this spatial point are given in Fig. 4a. The intensities above 63% of the I_{max} were then selected with the resulting beam shown in Fig. 4b and represented as the threshold mask, $Mask_{TR}$. This process was repeated for each scenario. It is worth noting that threshold value did not fluctuate significantly from one experimental condition to the other.

Using $Mask_{TR}$ we find $SI_{TR} = SI_B . * Mask_{TR}$. To obtain a single parameter representing SI we find the average value MSI_{TR}:

$$MSI_{TR\,avg} = \frac{\sum_{k=1}^{n} \sum_{j=1}^{m} SI_{TR\,j,k}}{nm} \tag{7}$$

Figure 5 shows a typical distribution of the scintillation index calculated for each pixel, as a function of measured camera light intensity (non-normalized). The intensity threshold is clearly noticeable along with the un-correlated distribution. During the testing, the intensity of the light on the camera sensor was kept constant (nearmiddle of the full camera range) by the use of neutral density filters.

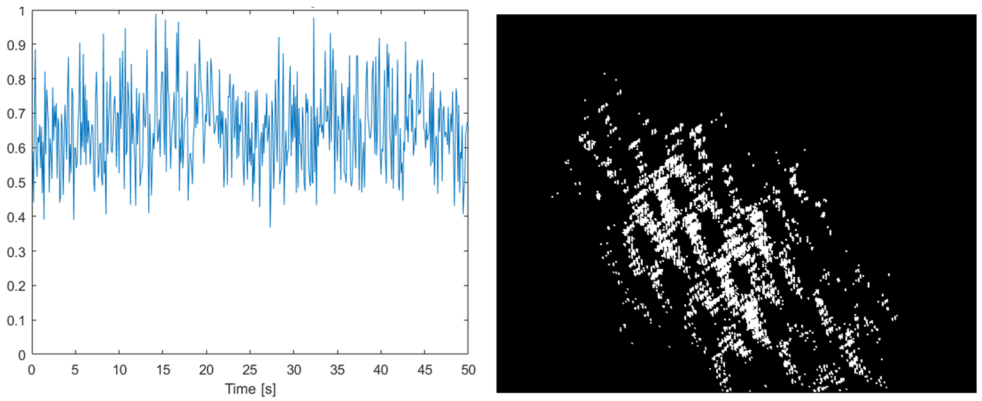

Fig. 4. a) SG beam light intensity fluctuations after propagating underwater with mechanical agitation at the pixel location of the maximum intensity I_{max}, as determined form I_{avg}. b) Selected area for analysis $Mask_{TR}$.

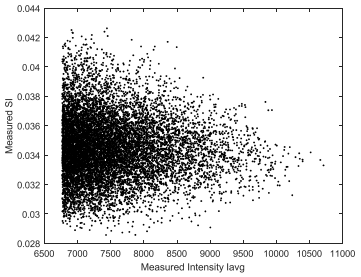

Fig. 5. Dependence of the scintillation index SI_B on the measured light intensity I_{avg} for the selected analysis area. Conditions were for an SG beam with $\delta = 0.38$ mm propagating in calm water.

5. Results

The experiments were carried out in two underwater conditions: propagation through calm water and mechanically agitated water. In the first step, a Gaussian beam was propagated and the intensity fluctuations were recorded in order to establish a baseline result for comparison of an increased scintillation index from calm to mechanically agitated conditions. Figure 6 shows the mean intensity I_{avg} distribution across the sensor area and demonstrating a notable beam spreading between calm and mechanically agitated conditions. Figure 7 shows the dependence of the scintillation index SI_B on the measured light intensity, clearly indicating the trend of an increased (from Fig. 7a to Fig. 7b) mean scintillation $MSI_{TR\ avg}$ from 0.0022 in the case of the calm water to 0.0091 in the case of agitated water - a rise of 61%.

Figure 8 highlights the trend of higher scintillation in turbulent water for both sets of beams. It is important to note that spatially partially coherent beams have higher scintillation, as compared to the Gaussian baseline (as can be seen from the calm scintillation index), resulting from the finite screen cycling rates due to equipment that is practically available for beam generation. While absolute scintillation indices are not practically obtainable, the relative scintillations indices are compared.

Table 1 presents the summary of the experimental results. Low standard deviation of the measured scintillation index across selected area of analysis confirms reliable experimental data

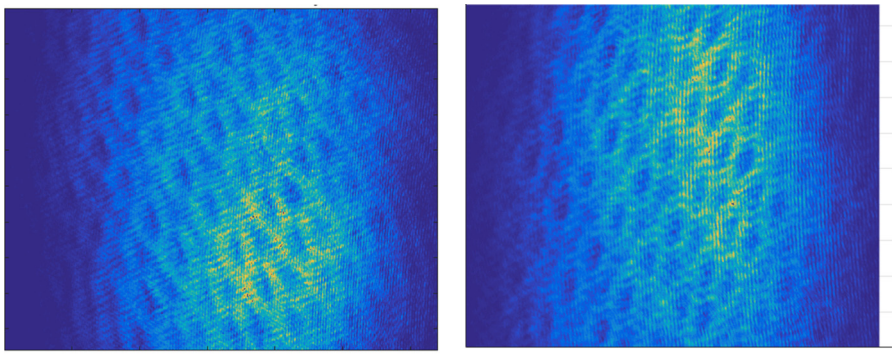

a) b)

Fig. 6. Gaussian beam mean intensity I_{avg} distribution across the sensor area propagating through a) calm and b) mechanically agitated water. Sensor area (3.552 mm × 4.736 mm).

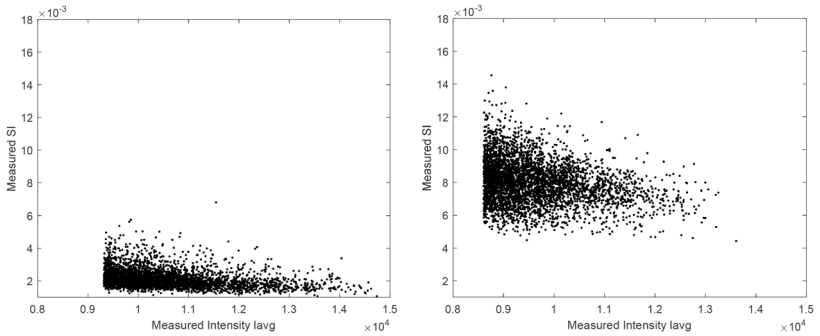

Fig. 7. Dependence of the scintillation index SI_B on the measured light intensity I_{avg} for Gaussian beam propagating through a) calm and b) mechanically agitated water.

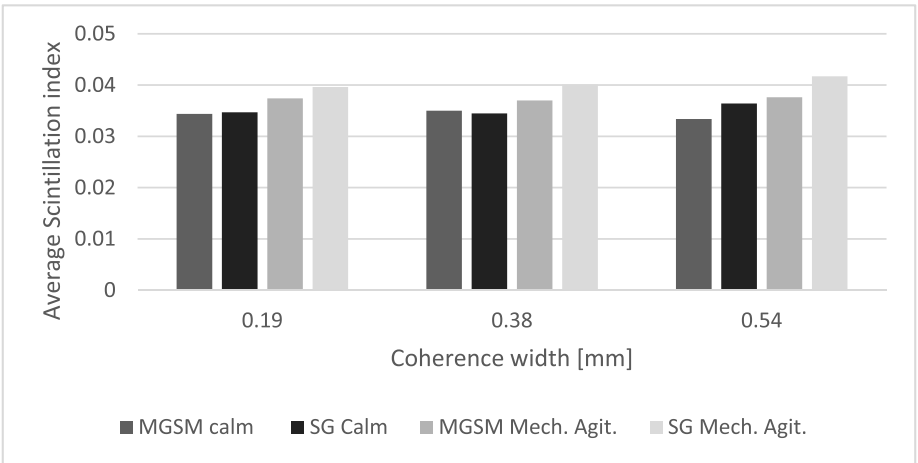

Fig. 8. Measured average scintillation indices for calm and mechanically agitated conditions for MGSM and SG beams.

OSA CONTINUUM

Table 1. Summary of the experimental results

Average scintillation index, $MSI_{TR\ avg}$ ± Standard deviation of the measurements						
R.M.S Correlation Width, δ	Beam type	Water condition		Beam type	Water condition	
		Calm	Mechanically Agitated		Calm	Mechanically Agitated
0.19 mm	MGSM	0.0344 ± 0.0030	0.0374 ± 0.0030	SG	0.0347 ± 0.0022	0.0396 ± 0.0030
0.38 mm		0.0350 ± 0.0023	0.0370 ± 0.0024		0.0345 ± 0.0021	0.0401 ± 0.0027
0.54 mm		0.0334 ± 0.0026	0.0376 ± 0.0027		0.0364 ± 0.0036	0.0417 ± 0.0030

set. Note that δ was defined in Eq. (1) as the r.m.s. width of the degree of coherence; it is labelled as the coherence width in the figures and tables.

Additionally, the experimental set up provided laser light intensity fluctuations measurements just before the beam entered the water tank which allowed the SG and MGSM beam classes to be compared as a function solely of the random media. Figure 9a shows the percentage of increase in the measured averaged scintillation indices for partially coherent beams with varying degrees of spatial coherence in scenarios (mechanically agitated vs. calm and air for both MGSM and SG beams). There is a clear trend indicating that SG beams have a reduced scintillation index performance compared with MGSM beams when going from calm to agitated conditions for all tested r.m.s. degrees of coherence width. Additionally, there appears to be a noticeable decrease in performance of the SG beam scintillation index when propagating from air to mechanically agitated water (~11–13% increase). As described earlier, the Gaussian beam (see Fig. 9b) was propagated solely as a baseline – the absolute scintillation measure of the Gaussian is not readily comparable to the experimentally generated PPCBs due to the physical cycling of the SLM equipment, which adds an additional mechanically elevated scintillation component - and showed similar poor performance with an approximately 90% increase in scintillation index going form air to mechanically agitated conditions. This as compared, for example, with the MGSM (~6-10%) and SG (11-13%).

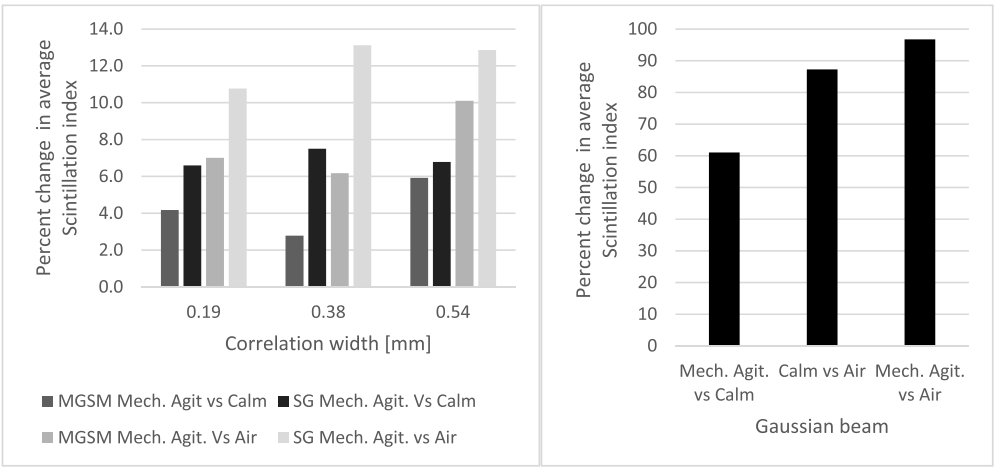

a) b)

Fig. 9. Percent increase in scintillation for MGSM, SG, and Gaussian beams under air, air + calm water, and air + mechanically agitated conditions.

OSA CONTINUUM

6. Conclusions

We investigated the propagation of spatially partially coherent SG and MGSM beams underwater under two conditions—calm and mechanically agitated water. In the case of scintillation index, MGSM beams appear to perform significantly better than SG beams under all tested scenarios. To our knowledge, this paper is the first to report experimental results of partially spatially coherent beams propagating through underwater turbulence. It represents a necessary first step before partially coherent beams can be applied in real-world applications such as underwater optical communications and remote sensing.

Funding

Office of Naval Research (ONR) (N0001414-WX-00267).

Acknowledgments

S. Avramov-Zamurovic is supported by US ONR grant: N0001414-WX-00267.

References

1. L. C. Andrews and R. L. Phillips, *Laser Beam Propagation through Random Media*, 2nd ed. (SPIE Press, 2005).
2. A. Ishimaru, *Wave Propagation and Scattering in Random Media*, vols. 1 and 2, (Academic, 1978).
3. F. Wang, X. Liu, and Y. Cai, "Propagation of partially coherent beam in turbulent atmosphere: a review (invited review)," Prog. Electromagn. Res. **150**, 123–143 (2015).
4. V. A. Banakh and V. M. Buldakov, "Effect of the initial degree of spatial coherence of a light beam on intensity fluctuations in a turbulent atmosphere," Opt. Spectrosc. **55**, 707–712 (1983).
5. J. C. Ricklin and F. M. Davidson, "Atmospheric turbulence effects on a partially coherent Gaussian beam: implications for free-space laser communication," J. Opt. Soc. Am. A **19**(9), 1794–1802 (2002).
6. J. H. Churnside, "Aperture averaging of optical scintillations in the turbulent atmosphere," Appl. Opt. **30**(15), 1982–1994 (1991).
7. S. Rosenberg and M. C. Teich, "Photocounting array receivers for optical communication through the lognormal atmospheric channel 2: optimum and suboptimum receiver performance for binary signaling," Appl. Opt. **12**(11), 2625–2634 (1973).
8. E. J. Lee and V. W. S. Chan, "Part 1: optical communication over the clear turbulent atmospheric channel using diversity," IEEE J. Select. Areas Commun. **22**(9), 1896–1906 (2004).
9. G. P. Berman, A. R. Bishop, B. M. Chernobrod, D. C. Nguyen, and V. N. Gorshkov, "Suppression of intensity fluctuations in free space high-speed optical communication based on spectral encoding of a partially coherent beam," Opt. Commun. **280**(2), 264–270 (2007).
10. G. P. Berman and A. A. Chumak, "Influence of phase-diffuser dynamics on scintillations of laser radiation in Earth's atmosphere: long-distance propagation," Phys. Rev. A **79**(6), 063848 (2009).
11. O. Korotkova, "Scintillation index of a stochastic electromagnetic beam propagating in random media," Opt. Commun. **281**(9), 2342–2348 (2008).
12. Y. Gu, O. Korotkova, and G. Gbur, "Scintillation of nonuniformly polarized beams in atmospheric turbulence," Opt. Lett. **34**(15), 2261–2263 (2009).
13. X. Xiao and D. Voelz, "Wave optics simulation of partially coherent and partially polarized beam propagation in turbulence," *Proc. SPIE 7464, Free-Space Laser Communications IX*, 74640 T; Aug 21; San Diego, CA. (2009).
14. S. Avramov-Zamurovic, C. Nelson, R. Malek-Madani, and O. Korotkova, "Polarization-induced reduction in scintillation of optical beams propagating in simulated turbulent atmospheric channels," Waves Random Complex Media **24**(4), 452–462 (2014).
15. F. Schill, U. R. Zimmer, and J. Trumpf, "Visible spectrum optical communication and distance sensing for underwater applications," *Proc. Australasian Conf. Robot. Autom.*, (2004).
16. N. Farr, J. Ware, C. Pontbriand, T. Hammar, and M. Tivey, "Optical communication system expands CORK seafloor observatory's bandwidth," *Proc. OCEANS Conf.* (2010).
17. M. Doniec, C. Detweiler, I. Vasilescu, and D. Rus, "Using optical communication for remote underwater robot operation," *IEEE/RSJ International Conference on Intelligent Robots and Systems* (2010).
18. B. Cochenour, A. Laux, and L. Mullen, "Temporal dispersion in underwater laser communication links: Closing the loop between model and experiment," *Proceedings Underwater Communications and Networking Conference (UComms)*, IEEE Third, (2016).
19. O. Korotkova, N. Farwell, and E. Shchepakina, "Light scintillation in oceanic turbulence," Waves Random Complex Media **22**(2), 260–266 (2012).
20. Y. Wu, Y. Zhang, and Y. Zhu, "Average intensity and directionality of partially coherent model beams propagating in turbulent ocean," J. Opt. Soc. Am. A **33**(8), 1451–1458 (2016).

OSA CONTINUUM

21. H. Lajunen and T. Saastamoinen, "Propagation characteristics of partially coherent beams with spatially varying correlations," Opt. Lett. **36**(20), 4104–4106 (2011).
22. Y. Gu and G. Gbur, "Scintillation of nonuniformly correlated beams in atmospheric turbulence," Opt. Lett. **38**(9), 1395–1397 (2013).
23. Y. Cai, Y. Chen, and F. Wang, "Generation and propagation of partially coherent beams with nonconventional correlation functions: a review [Invited]," J. Opt. Soc. Am. A **31**(9), 2083–2096 (2014).
24. O. Korotkova, S. Sahin, and E. Shchepakina, "Multi-Gaussian Schell-model beams," J. Opt. Soc. Am. A **29**(10), 2159–2164 (2012).
25. G. Gbur and T. D. Visser, "The structure of partially coherent fields," Prog. Opt. **55**, 285–341 (2010).
26. S. Sahin and O. Korotkova, "Light sources generating far fields with tunable flat profiles," Opt. Lett. **37**(14), 2970–2972 (2012).
27. M. W. Hyde IV, S. Basu, X. Xiao, and D. Voelz, "Producing any desired far-field mean irradiance pattern using a partially-coherent Schell-model source," J. Opt. **17**(5), 055607 (2015).
28. M. W. Hyde, S. Basu, X. Xiao, and D. G. Voelz, "Producing any desired far-field mean irradiance pattern using a partially-coherent Schell-model source and phase-only control," *Imaging and Applied Optics 2015 OSA Technical Digest* (online) (Optical Society of America), paper PW3E.2. (2015).
29. M. W. Hyde, S. Basu, D. G. Voelz, and X. Xiao, "Experimentally generating any desired partially coherent Schell-model source using phase-only control," J. Appl. Phys. **118**(9), 093102 (2015).
30. S. Avramov-Zamurovic, C. Nelson, S. Guth, and O. Korotkova, "Flatness parameter influence on scintillation reduction for multi-Gaussian Schell-model beams propagating in turbulent air," Appl. Opt. **55**(13), 3442–3446 (2016).
31. C. Nelson, S. Avramov-Zamurovic, O. Korotkova, S. Guth, and R. Malek-Madani, "Scintillation reduction in pseudo Multi-Gaussian Schell Model beams in the maritime environment," Opt. Commun. **364**, 145–149 (2016).
32. S. Avramov-Zamurovic and C. Nelson, "Experimental study on off-axis scattering of flat top partially coherent laser beams when propagating under water in the presence of moving scatterers," Waves Random Complex Media **28**(4), 743–759 (2018).